IEEE Access
Multidisciplinary | Rapid Review | Open Access Journal

Received April 18, 2018, accepted May 26, 2018, date of publication June 5, 2018, date of current version June 26, 2018.

Digital Object Identifier 10.1109/ACCESS.2018.2844164

Modeling and Experimental Validation of the Time Delay in a Pilot Operated Proportional Directional Valve

JUNHUI ZHANG[1], DI WANG[1], BING XU[1], ZHENYU LU[1], MINYAO GAN[2], AND Qi SU[3]

[1]State Key Laboratory of Fluid Power and Mechatronic Systems, Zhejiang University, Hangzhou 310027, China
[2]Shanghai Marine Equipment Research Institute, Shanghai 200031, China
[3]School of Mechanical Engineering, Zhejiang University, Hangzhou 310027, China

Corresponding author: Bing Xu (bxu@zju.edu.cn)

This work was supported in part by the NSFC-Zhejiang Joint Fund for the Integration of Industrialization and Informatization under Grant U1509204, in part by the National Natural Science Foundation of China under Grant 91748210, and in part by the National Basic Research Program of China (973 Program) under Grant 2014CB046403.

ABSTRACT The pilot-operated proportional directional valve is a crucial component in the airplane landing gear retraction system. The time delay of the proportional valve directly affects the retraction behavior even the flight safety and needs to be analyzed. Therefore, the modeling and analysis of a typical pilot-operated proportional directional valve are presented in this paper. Substantially, the nonlinear valve system is composed of four subsystems: mechanical, electronic, electromagnetic, and fluid dynamic subsystems. The subsystems are modeled based on a lumped parameter approach. The coupling among the subsystems is analyzed. The nonlinearity is implemented using a specific set of equations in the model. Especially, the nonlinearity observed in practical application is considered in modeling the effect of the electronic anti-unloading power drive circuit on the pulse-width modulation signal. The analytical results of the model show good agreement with the experimental ones. The investigation shows that the delay of the valve results from multiple subsystems' dynamic performances which act sequentially on the main spool. The effect of the electronic part and the structural part is analyzed, and the proportion of each part is given based on the simulation results. The analysis shows that the model can provide a direct suggestion in choosing the valve part to optimize and the optimization effect limit.

INDEX TERMS Aerospace engineering, electrohydraulics, modeling, proportional directional valve, time delay.

I. INTRODUCTION

The landing gear is a key structure which supports airplanes on the ground and is used to help airplanes taxi, take off and land. Though it is quite crucial for the airplanes on the ground, it acts as a barrier of the air during the flight. Therefore, most airplanes retract the landing gear in the air to improve the performance [1]. With the progress in the airplane, the landing gear is required to retract as quickly as possible to improve the climbing speed [2]. The position changing operation needs to be implemented in seconds [3]. Although the electro-hydrostatic actuator (EHA) is used in the aircraft as local electrically powered actuation systems [4], [5], the electronic pilot operated proportional directional valves are still widely used in the hydraulic controlling system considering the robustness and the velocity requirement of the landing gear retraction system [6], [7]. The proportional directional valves are less sensitive to contamination but respond slower than the servo valves. The mechanical, electronic, electromagnetic, and fluid dynamic subsystems in the proportional valve realize the function of controlling the spool position proportionally to the signal provided to the solenoid. However, the complex coupling of the above subsystems also complicates the valve analysis and many researchers have paid much effort to analyze the limit factors and shorten the valve response time.

For the mechanical subsystem, friction and dead band were found in the simulation and experiments to delay the valve response, cause oscillation and even the instability of the close-loop system if they are not been properly dealt with [8]–[13]. Besides improving the machining

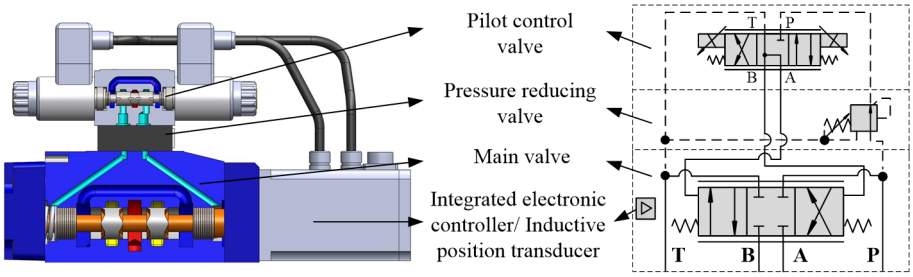

FIGURE 1. Structure of the pilot operated proportional directional valve.

and assembling technology to reduce the delay effect, novel structures of replacing the pilot directional valve with the digital pressure valve and the proportional pressure reducing valve were also proposed [14], [15]. These structures reduced the side effect of the friction and the dead band by changing the pilot valve function. For the electronic subsystem, the eddy current effect was analyzed and different electronic circuit structures were proposed to shorten the response time. For example, Breidi *et al.* [16] proposed peak-and-hold and reverse current driving strategies, and the electronic circuit was modified to tolerate the extra high supply voltage so that the eddy current, the coil inductance, and the valve response delay could be reduced. Lee [17] brought up a novel three-power-source-type valve driving circuit based on similar consideration. For the electromagnetic subsystem, the flux linkage related to structural parameters was looked into and some methods were proposed for the design and the control strategy of the solenoid. For instance, Davide and Andrea simulated the solenoid using a finite element analysis (FEA) three-dimensional model, and compared the performance of the nonlinear model with the linearized one [18]. Kong and Li [19] built a differential model to analyze the effect of multiple coils, and proposed a parallel-coil solenoid to accelerate the spool. Zhu and Jin [20] proposed a nonlinear solenoids model using a interpolation method and combined it with the linearized mechanical model to simulate the proportional directional valve. Jin *et al.* [21] also used a two-dimensional interpolation method to model the solenoid and proposed a differential control method to use both solenoids of the proportional directional valve for fast direction switching. For the fluid dynamic subsystem, effort was paid on reducing the flow force. For instance, Amirante *et al.* [22] optimized the spool using computational fluid dynamics (CFD) methods and genetic algorithm so that the flow force can be reduced. Similar researches for flow force reduction were also carried out by adjusting the structural parameters of the spool or the sleeve [23]–[25].

As stated above, the four subsystems are coupled together, and researches were carried out to look into the interactions. For example, Meng *et al.* [26] paid much attention to the coupling relationship between the valve subsystems and used a feedback loop iteration procedure to analyze the coupling. Yang *et al.* [9] used the Bond graphs to reveal the interaction within a proportional pressure control valve. However, although many researches focused on the system interaction, some subsystems were usually simplified. Meng *et al.* [26] simplified the electronic circuit as a proportional function, and Yang *et al.* [9] simplified the compression force delay with a constant delay link. Fang *et al.* [27] and Canuto and Bravo [28] linearized the entire valve model and applied advanced control strategies to compensate the nonlinearity. Vaughan and Gamble [29] and Dell'Amico and Krus [30] both proposed a fitting model based on the measured data of a nonlinear proportional solenoid valve, and they also simplified the electronic circuit model.

Many researchers who study the coupling of the proportional valves linearize the subsystems to simplify control and optimization. However, the loss of nonlinearity affects the detailed behavior of the valve models, especially the dynamic behavior. Since the proportional directional valve has four subsystems coupled with each other, it is important to keep the main nonlinear factors of each subsystem so that the chain reaction caused by the nonlinearity can be simulated. Therefore, the main nonlinearity of each subsystem is maintained in our simulation and the proportion of delay caused by each subsystem is analyzed. The model can not only be used as a tool to simulate the valve response, but also give a direct suggestion in choosing the valve part to optimize.

In this paper, a lumped parameter (LP) model of the four subsystems in the proportional directional valve is proposed. The nonlinearity in the electronic circuit, the solenoid, and the spool movement are analyzed and presented. The analysis is focused on the main stage spool position of the valve instead of the pressure or the flow which can be influenced by the hydraulic circuit. The results of the overall simulation model are verified by experiments, and the proportion of the effect that the subsystems have on the time delay is analyzed.

II. VALVE STRUCTURE AND OPERATION PRINCIPLE

The proportional directional valve in this research is a typical pilot operated proportional directional valve which adjusts the main stage spool position according to the input. The structure of the valve is presented in Fig. 1. The pilot operated proportional directional valve consists of an integrated electronic controller, a pilot control valve, a pressure reducing valve, a main valve, an inductive position transducer, and

other components. The electronic controller consists mainly of an amplifier, a digital microprocessor, and an I/O interface. The pilot valve is a three-position four-port proportional directional valve in which the spool position is proportionally controlled by the solenoids. The ports A and B of the pilot valve are connected with the T port when the spool is at the central position, and the main spool is forced to slide back to the central position by the centering spring at this time. The pressure reducing valve is used to stabilize the supply pressure for the pilot valve so that the effect of the external pressure can be reduced. The main valve is a three-position four-port proportional directional valve and the spool is driven by the pilot pressure. The inductive position transducer measures the actual main spool position and forms a closed loop spool position controller.

When there is no input signal, the pilot spool and the main spool are kept in the central positions by the centering springs. When the valve is given a control signal, the main spool position measured by the inductive transducer is compared with the signal and a differential voltage is created. Then the electronic circuit adjusts the duty cycle of the pulse-width modulation (PWM) control signal so that the solenoid is driven by the corresponding current. The current produces force in the solenoid and moves the pilot spool. The pilot flow changes with the pilot spool position variation and adjusts the main spool position. Then the main spool can be driven to the desired position to realize flow and direction control function. Since the control process is affected by all the subsystems, the coupled nonlinear model needs to be built for detailed analysis.

III. PILOT OPERATED PROPORTIONAL DIRECTIONAL VALVE MODELING

Because the subsystems are coupled severely, the valve modeling procedure is divided into four parts. The mechanical subsystem, the electronic subsystem, the electromagnetic subsystem, and the fluid dynamic subsystem are modeled separately. The nomenclature and the value of the parameters are presented in Table 1.

A. MECHANICAL SUBSYSTEM MODELING

The mechanical subsystem presents the forces acting on the spools and predicts the dynamic behavior of the valve. The other subsystems are coupled with each other by forces in the mechanical subsystem and affect the spool position. Therefore, the mechanical subsystem is modeled firstly to reveal the relationship among the subsystems.

The pilot operated proportional directional valve is composed of the pilot stage proportional directional valve and the main stage proportional directional valve. The situation that the pilot spool moving to the right and the main spool moving to the left is taken for example and the forces acting on the spools are presented in Fig. 2.

The pilot stage proportional directional valve is driven by the magnetic force F_{m}, and the Newton's second law is used

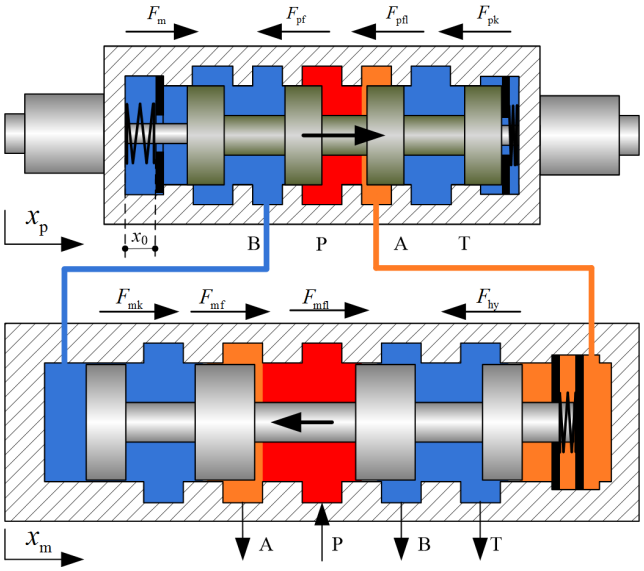

FIGURE 2. Schematic of the forces acting on the spools.

to model the pilot valve as

$$F_{\mathrm{m}} = m_{\mathrm{p}}\ddot{x}_{\mathrm{p}} + b_{\mathrm{p}}\dot{x}_{\mathrm{p}} + F_{\mathrm{pk}} + F_{\mathrm{pfl}} + F_{\mathrm{pf}}\mathrm{sgn}\left(\dot{x}_{\mathrm{p}}\right) - x_{\mathrm{p\,max}} \le x_{\mathrm{p}} \le x_{p\,\mathrm{max}}, \quad (1)$$

where m_{p} is the total mass, b_{p} is the viscous coefficient, x_{p} is the displacement of the pilot spool, F_{pk} is the spring force, F_{pfl} is the flow force, F_{pf} is the Coulomb friction, and x_{pmax} is the stroke of the pilot valve spool. The static friction is ignored because of the dither signal given to the solenoids. The Coulomb friction and the viscous coefficient can be calculated based on the force and velocity data when the oil is just used for lubrication [27]. Based on the structure of the pilot valve, the spring force can be expressed using the piecewise function as

$$F_{\mathrm{pk}} = \begin{cases} \left(2k_{\mathrm{p}}x_{\mathrm{p}}\right)\mathrm{sgn}\left(x_p\right) & 0 \le \left|x_p\right| < x_0, \\ \left(k_{\mathrm{p}}x_{\mathrm{p}} + F_{\mathrm{pk0}}\right)\mathrm{sgn}\left(x_p\right) & x_0 \le \left|x_p\right| \le x_{max}, \end{cases} \quad (2)$$

where k_{p} is the elastic coefficient of the spring, F_{pk0} is the spring preload, and x_0 is the structure limited stroke. When the displacement is smaller than x_0, the left spring and the right spring act on the spool together, and when the displacement is larger than x_0, one spring is blocked by the structure and cannot act on the spool. The structural parameter x_0 is also presented in Fig. 2.

The main stage proportional directional valve can also be modeled by considering the Newton's second law and the coupling relationship between the main spool and the pilot pressure [31]. The main spool motion can be modeled as

$$F_{\mathrm{hy}} = M\ddot{x}_{\mathrm{m}} + b_{\mathrm{m}}\dot{x}_{\mathrm{m}} + F_{\mathrm{mk}} + F_{\mathrm{mfl}} + F_{\mathrm{mf}}\mathrm{sgn}\left(\dot{x}_{\mathrm{m}}\right) - x_{\mathrm{m\,max}} \le x_m \le x_{\mathrm{m\,max}}, \quad (3)$$

where F_{hy} is the pilot pressure force acting on the main spool, M is the total moving mass of the main stage proportional

directional valve, x_m is the displacement of the main spool, b_m is the viscous coefficient, F_{mk} is the spring force, F_{mfl} is the flow force of the main spool, F_{mf} is the friction force, and x_{mmax} is the stroke of the main stage spool. The spring force acting on the main spool can be expressed as

$$F_{mk} = (k_m |x_m| + F_{mk0}) \operatorname{sgn}(x_m)\, 0 \le |x_m| \le x_{m\max}, \quad (4)$$

where k_m is the spring elastic coefficient and F_{mk0} is the spring preload. The friction force F_{mf} is a combination of the static friction and the Coulomb friction. The friction forces are measured based on the pressure differential of the control chambers with no oil flowing through the main spool. In order to measure the maximum static friction, a small signal is given to the pilot valve to move the main spool slightly in each direction. Because of the tiny displacement change, the spring force can be viewed as unchanged, and the only change is the static friction's direction. The subtraction of the force equations when the spool moves in each direction can eliminate the spring force and lead to the maximum static friction value [32]. The Coulomb friction and the viscous coefficient can also be calculated based on the pressure differential and velocity data of the main spool using the same method as the one used in the pilot valve.

From the model, it can be obtained that the forces generated by each subsystem act simultaneously on the spools. In the pilot valve, the main driving force is the electromagnetic force and the main resistance forces are the flow force and spring force. And in the main valve, the main driving force is the pilot pressure force caused by the pressure differential. The flow force and the spring force also act as the main resistance forces. Detailed modeling of the electronic, the electromagnetic, and the fluid dynamic subsystems are needed to reflect the dynamic behavior of the valves.

B. ELECTRONIC SUBSYSTEM MODELING

Electronic circuit converts the control signal to the supply current. It adjusts the duty cycle of the PWM correspondingly to the control signal and generates the control current in the solenoid circuit. Because of the fast response of the electronic circuit, the circuit is usually viewed as a proportional function between the signal and the current [21], [26], [33]. However, in the anti-unloading power drive circuit used in current situation, the fast unloading causes the reverse voltage which couples with the solenoid current. Therefore, the feature of the anti-unloading power drive circuit needs to be analyzed and modeled.

The schematic of the anti-unloading power drive circuit in use is presented in Fig. 3. An optocoupler is used to separate the control signal with the driving circuit and resistors are used to control the field effect transistors with the same PWM signal. When the PWM signal is high, the two field effect transistors open simultaneously and the supply voltage is applied to the solenoid and generates the driving current. When the PWM signal is low, the two field effect transistors shut down simultaneously and the reverse voltage is applied to the solenoid for restraining the inductive current.

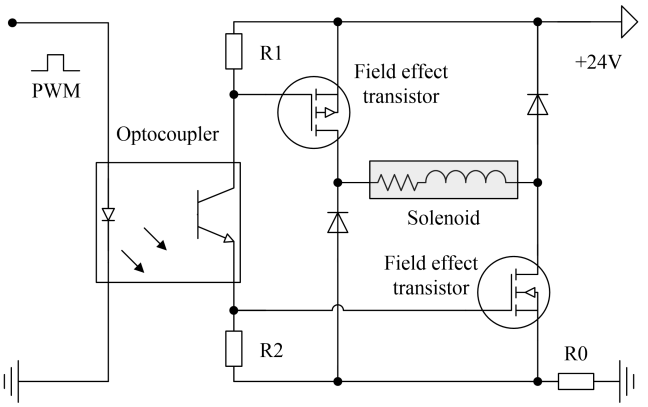

FIGURE 3. The schematic of the anti-unloading power drive circuit.

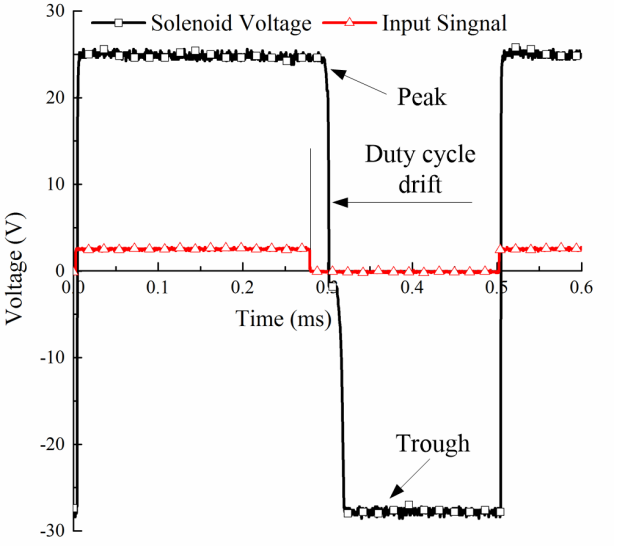

FIGURE 4. The experimental behavior of the anti-unloading power drive circuit.

The circuit is tested with the signal of 3.3 V and the standard rectangular PWM signal of 2000 Hz with the duty cycle of 55%. The test results are presented in Fig. 4. From the results, it can be found that there exist two irregular points that need to be considered in the modeling. The first point is the duty cycle drift. The delay of the optocoupler causes the larger proportion of the high voltage period in the entire cycle than the desired duty cycle. The shutting delay of the optocoupler is about 26 μs. Therefore, the circuit and the field effect transistors are not shut immediately but are delayed by the optocoupler. The second point is the asymmetrical voltage supply. The circuit difference and the related electronic components lead to different voltage values acting on the solenoid when the PWM signal is high and low. Therefore, it can be concluded that the anti-unloading power drive circuit cannot be simplified as the ideal proportional function, and the nonlinear characteristics need to be considered in the modeling.

The duty cycle of the actual PWM signal is modified with the time delay caused by the optocoupler and the field effect transistors. Therefore, the modified duty cycle can be expressed as

$$D_{\text{out}} = \begin{cases} 0 & D_{\text{c}} = 0, \\ D_{\text{c}} + t_{\text{d}} f_{\text{p}} & 0 < D_{\text{c}} + t_{\text{d}} f_{\text{p}} \leq 1, \\ 1 & D_{\text{c}} + t_{\text{d}} f_{\text{p}} > 1, \end{cases} \tag{5}$$

where D_{out} represents the output duty cycle, D_{c} represents the control duty cycle, t_{d} represents the time delay, and f_{p} is the frequency of the PWM signal. The output duty cycle is limited since the duty cycle needs to be contained within one.

Because of the asymmetrical voltage observed in the experiments, the output voltage is modeled separately at the different stages of the PWM signal. The piece-wise function is presented as

$$u_{\text{out}}(t) = \begin{cases} u_{\text{on}}(t) & kT < t \leq kT + D_{\text{c}}T + t_{\text{d}}, \\ u_{\text{off}}(t) & kT + D_{\text{c}}T + t_{\text{d}} < t \leq kT + T, \end{cases} \tag{6}$$

where u_{out} is the output voltage, u_{on} is the voltage when the PWM is high and u_{off} is the voltage when the PWM is low, T is the cycle of the PWM signal. The electronic circuit is simplified separately when the PWM signal is high and low to calculate the corresponding voltage in (6) and is presented in Fig. 5.

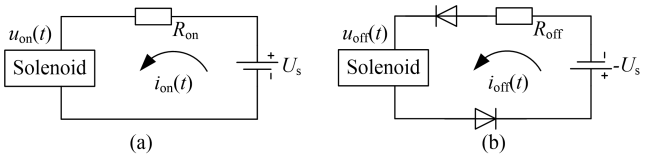

FIGURE 5. Simplified electronic circuit: (a) when the PWM signal is high (b) when the PWM signal is low.

When the PWM signal is high, the resistances in the circuit except the solenoid, such as the resistance of the field effect transistors and the resistor R0, are combined together and equivalent to resistance R_{on}. The function of the voltage and the current can be expressed as

$$u_{\text{on}}(t) = U_{\text{s}} - i_{\text{on}}(t) R_{\text{on}}, \tag{7}$$

where U_{s} is the supply voltage of the power source and i_{on} is the current in the circuit.

When the PWM signal is low, the resistances in the circuit, such as the resistance in the diodes and the resistor R0, are also combined together and equivalent to resistance R_{off}. Then the voltage can be expressed as (8).

$$u_{\text{off}}(t) = \begin{cases} -U_{\text{s}} - i_{\text{off}}(t) R_{\text{off}} & i_{\text{off}}(t) > 0, \\ 0 & i_{\text{off}}(t) = 0. \end{cases} \tag{8}$$

C. ELECTROMAGNETIC SUBSYSTEM MODELING

The electromagnetic subsystem is quite important for transferring the electronic signal to force and driving the spool. To model the nonlinear solenoid characteristics precisely, the core position and the driving voltage are taken into consideration. The solenoid is modeled as an inductor in parallel with a dissipative resistor and then connected with a resistor in series. The simplified schematic of the solenoid is expressed in Fig. 6, where u_{s} is the voltage on the solenoid, L is the nonlinear inductor which is defined by the magnetic material outside the coil, the core material, the air gap. The inductor value is affected by the flux linkage λ and the core position x_{p} and can be presented as $L(\lambda, x_{\text{p}})$. R represented the resistance of the coil, which depends on the coil material, length, cross section area, and temperature. Since the experiments are carried out under the room temperature in the same season and the time is kept short, the resistance is viewed as a constant. R_{d} represents the dissipative resistor which is affected by the inductive voltage u_{L} and the core position x_{p}. The dissipative resistance is highly nonlinear and the value can be presented as $R_{\text{d}}(u_{\text{L}}, x_{\text{p}})$.

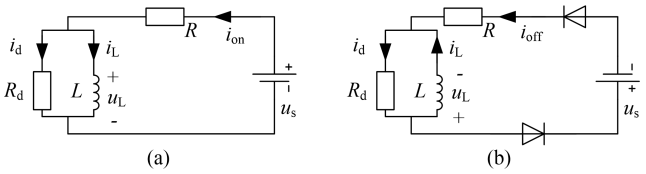

FIGURE 6. The simplified schematic of the solenoid: (a) when $u_{\text{s}} \geq 0$ (b) when $u_{\text{s}} < 0$.

The total voltage over the solenoid can be expressed as

$$u_{\text{s}} = u_{\text{L}} + (i_{\text{d}} + i_{\text{L}}) R, \tag{9}$$

where u_{s} is the total voltage over the solenoid, i_{d} is the energy-dissipative current, and i_{L} is the energy-restoring current. From the law of electromagnetic induction, the inductive voltage u_{L} and energy-restoring current i_{L} can be expressed as

$$u_{\text{L}} = \frac{d\lambda}{dt} = \dot{\lambda}, \tag{10}$$

$$i_{\text{L}} = \frac{\lambda}{L(\lambda, x_{\text{p}})} = f(\lambda, x_{\text{p}})\lambda. \tag{11}$$

The energy-dissipative current i_{d} can be expressed as

$$i_{\text{d}} = \frac{u_{\text{L}}}{R_{\text{d}}(u_{\text{L}}, x_{\text{p}})} = \frac{u_{\text{L}}}{R_{\text{d}}(\dot{\lambda}, x_{\text{p}})} = g(\dot{\lambda}, x_{\text{p}}) u_{\text{L}}. \tag{12}$$

The relationship between the total voltage u_{s} and the flux linkage λ can be calculated by combining (9) and (12) as

$$u_{\text{s}}(t) = (1 + g(\dot{\lambda}, x_{\text{p}}) R)\dot{\lambda} + f(\lambda, x_{\text{p}}) R\lambda. \tag{13}$$

The solenoid force is related to the square of flux linkage λ and the core position x_{p}, and can be expressed as

$$F_{\text{m}} = h(\lambda^2, x_{\text{p}}), \tag{14}$$

where F_{m} is the solenoid force [29]. From (13) and (14), the schematic of the nonlinear solenoid model can be deduced and is presented in Fig. 7. In the schematic, the three key

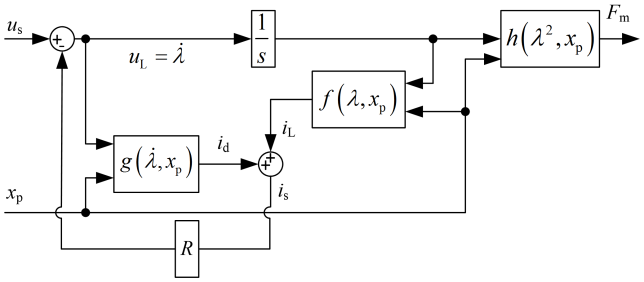

FIGURE 7. Schematic of the nonlinear solenoid model.

functions, $f(\lambda, x_p)$, $g(u_L, x_p)$, and $h(\lambda^2, x_p)$ are nonlinear and can be found by fitting polynomial functions [30].

The measurement is carried out using the step response measurement (SRM) method in which the core is fixed at certain positions and step signal is given for evaluating the magnetic system [34]. As an example, the solenoid voltage, the solenoid current, and the solenoid force when the solenoid is given 10 V step voltage and the core is fixed at 0 mm are presented in Fig. 8. Equations (9) and (10) are used to calculate the flux linkage λ and the magnetization curves are presented in Fig. 9. It can be seen from the magnetization curves that the hysteresis exists when the current increases or decreases. The restoring part is found using the mean current at each core position and is irrelevant with the current changing trend.

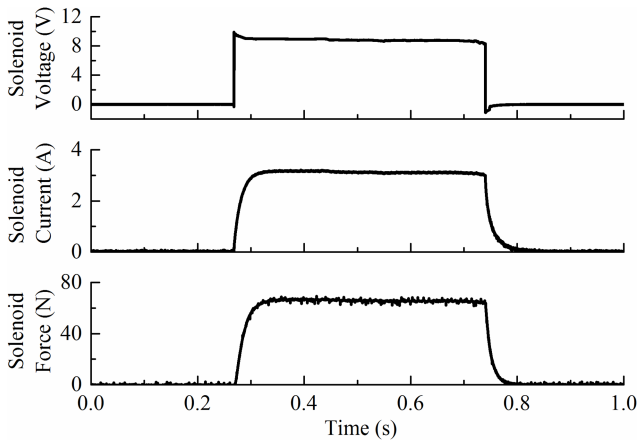

FIGURE 8. Behaviors of the solenoid when it is given step signal.

The flux linage λ is a monotonic function which passes the zero point. The fit is described by (15) to (17).

$$i_L = f(\lambda, x_p) = f_3(x_p)\lambda^3 + f_1(x_p)\lambda, \quad (15)$$

$$f_1(x_p) = f_{11}x_p + f_{10}, \quad (16)$$

$$f_3(x_p) = f_{33}x_p^3 + f_{32}x_p^2 + f_{31}x_p + f_{30}. \quad (17)$$

The dissipative current i_d and the inductive voltage u_L are presented in Fig. 10, in which the same changing

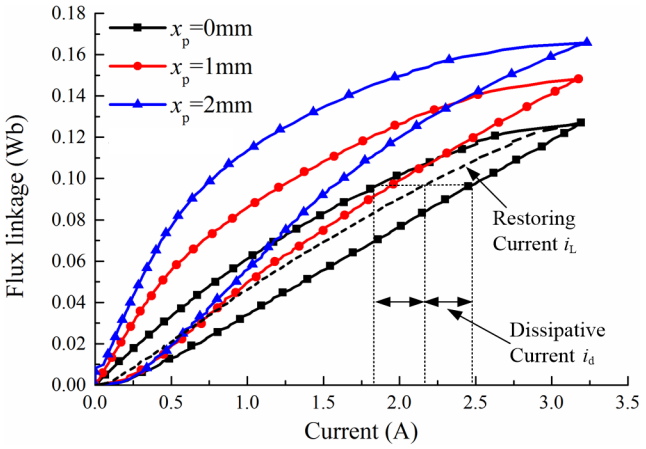

FIGURE 9. Flux linkage of the solenoid.

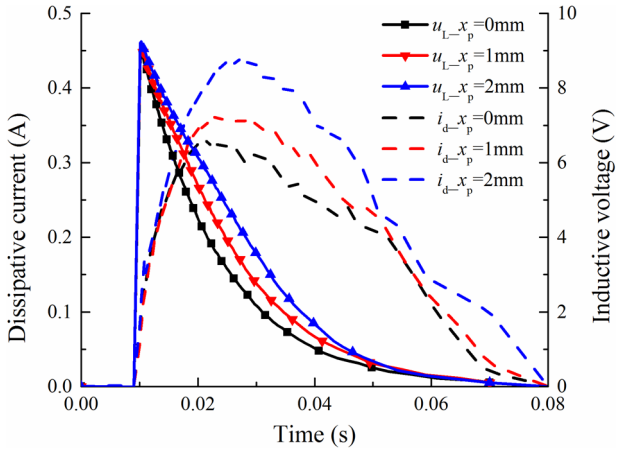

FIGURE 10. The dissipative current and the inductive voltage at different core positions when the solenoid is given step signals.

trend and typical delay can be observed in the current and voltage curves. Therefore, the model of the dissipative part is proposed by including a time constant to simulate the non-electrical hysteresis effects [29]. And the proposed one order inertial function is

$$i_d = \frac{K_s(x_p)}{T_s(x_p)} \exp\left(-\frac{1}{T_s(x_p)}t\right) u_L, \quad (18)$$

where $K_s(x_p)$ is the proportional coefficient and $T_s(x_p)$ is the time delay. The two functions are also fitted using the polynomial functions as follows.

$$K_s(x_p) = k_{s4}x_p^4 + k_{s3}x_p^3 + k_{s2}x_p^2 + k_{s1}x_p + k_{s0}. \quad (19)$$

$$T_s(x_p) = t_{s4}x_p^4 + t_{s3}x_p^3 + t_{s2}x_p^2 + t_{s1}x_p + t_{s0}. \quad (20)$$

The solenoid force is a function of the core position and the flux linkage, and the measured force at each core position is presented in Fig. 11. Though the hysteresis of the solenoid force is observed when the flux linkage changes, it is rather small and can be ignored. The mean solenoid force is

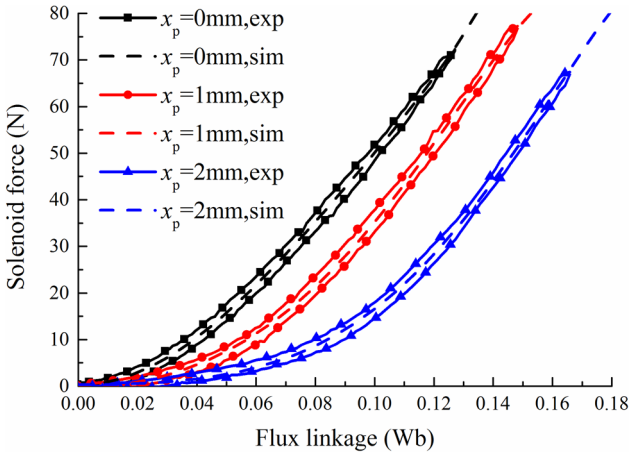

FIGURE 11. The solenoid force and the flux linkage at each position.

calculated and a polynomial model is fitted using (21) to (24).

$$F_m = h\left(\lambda^2, x_p\right) = h_3\left(x_p\right)\lambda^6 + h_2\left(x_p\right)\lambda^4 + h_1\left(x_p\right)\lambda^2, \tag{21}$$

$$h_1\left(x_p\right) = h_{13}x_p^3 + h_{12}x_p^2 + h_{11}x_p + h_{10}, \tag{22}$$

$$h_2\left(x_p\right) = h_{23}x_p^3 + h_{22}x_p^2 + h_{21}x_p + h_{20}, \tag{23}$$

$$h_3\left(x_p\right) = h_{33}x_p^3 + h_{32}x_p^2 + h_{31}x_p + h_{30}. \tag{24}$$

D. FLUID DYNAMIC SUBSYSTEM MODELING

The fluid dynamic subsystem converts the mechanical force to fluid performance. The electromagnetic force overcomes the viscous force, the spring force, the friction force, and the flow force in the pilot valve to move the pilot spool. The pressure differential acts on the valve opening and forces the oil to flow through the pilot spool. The resulting flow in the pilot stage proportional directional valve holds the spool from moving but drives the main spool to the desired position. The pressure differential acts on the main valve opening and gains the demanded flow. The viscous force, the spring force, the flow force, and the friction force in the main valve act against the pilot pressure force and balance the main spool. Therefore, the fluid dynamic subsystems in the pilot stage proportional valve and the main stage proportional valve are also modeled separately.

In the pilot stage, the flow results in the flow force as F_{pfl} in (1). In order to calculate the flow force, the flow through the orifices on the spool is defined as

$$q_p = C_q A_p \sqrt{\frac{2\Delta P_P}{\rho}}, \tag{25}$$

where q_p is the orifice flow rate, C_q is the discharge coefficient, A_P is the opening area, ΔP_P is the pressure differential over the orifice, and $\rho$is the oil density. Since the flow in the pilot stage valve can either be laminar or turbulent, the discharge coefficient is modeled by considering the flow state. The discharge coefficient is a function of the Reynolds number which represents the flow state [35]. The Reynolds number can be calculated by

$$\mathrm{Re} = \frac{\rho v d_h}{\upsilon} = \frac{4q}{S\eta}, \tag{26}$$

where Re is the Reynolds number, v is the oil velocity, d_h is the hydraulic diameter, υ is the dynamic viscosity, S is the perimeter of the orifice, and η is the kinematic viscosity. Although (26) is widely used to calculate the Reynolds number, the existence of flow q in the equation results in iteration in the calculation. To avoid the iteration, the flow number λ_h is used to replace the Reynolds number. The flow number is calculated by

$$\lambda_h = \frac{d_h}{\eta}\sqrt{\frac{2\left|\Delta P_p\right|}{\rho}}. \tag{27}$$

The discharge coefficient is calculated by the flow number using the equation

$$C_q = C_{tu}\tanh\left(\frac{2\lambda_h}{\lambda_{crit}}\right), \tag{28}$$

where C_{tu} is the discharge coefficient when the flow is fully developed turbulent, λ_{crit} is the critical flow number from the laminar flow to turbulent flow. C_{tu} is chosen to be 0.7 and λ_{crit} is chosen to be 100 [36], [37].

Another key factor in calculating the flow rate is the opening area of the pilot spool. The U-shape notch is used as the downstream opening of the pilot valve spool. Assuming that the number of the U-shape notches on each control edge is n_k, the opening area A_k can be expressed as

$$\begin{aligned} A_k &= f_a\left(n_k, R_u, y_k\right) \\ &= \begin{cases} 0 & y_k \le 0, \\ n_k R_u^2\left[\cos^{-1}\left(1-\dfrac{y_k}{R_u}\right)\right. & \\ \left. -\left(1-\dfrac{y_k}{R_u}\right)\sqrt{\dfrac{y_k}{R_u}\left(2-\dfrac{y_k}{R_u}\right)}\right] & 0 < y_k \le R_u, \\ n_k\left[\dfrac{\pi R_u^2}{2} + 2R_u\left(y_k - R_u\right)\right] & y_k > R_u, \end{cases} \end{aligned} \tag{29}$$

where R_u is the radius of the semi-circle and y_k is the axial length of the valve opening. Since the pilot spool is designed symmetrically, the dead zone of each port is assumed to be symmetrical too. The opening area of each orifice can be calculated by

$$\begin{aligned} A_{pb} &= \begin{cases} f_a\left(n_{pb}, R_u, -\Delta_2 - x_p\right) & -x_{p\max} \le x_p \le -\Delta_2, \\ 0 & \text{otherwise}, \end{cases} \\ A_{bt} &= \begin{cases} f_a\left(n_{bt}, R_u, \Delta_1 + x_p\right) & -\Delta_1 \le x_p \le x_{p\max}, \\ 0 & \text{otherwise}, \end{cases} \\ A_{at} &= \begin{cases} f_a\left(n_{at}, R_u, \Delta_1 - x_p\right) & -x_{p\max} \le x_p \le \Delta_1, \\ 0 & \text{otherwise}, \end{cases} \\ A_{pa} &= \begin{cases} f_a\left(n_{pa}, R_u, x_p - \Delta_2\right) & \Delta_2 \le x_p \le x_{p\max}, \\ 0 & \text{otherwise}, \end{cases} \end{aligned} \tag{30}$$

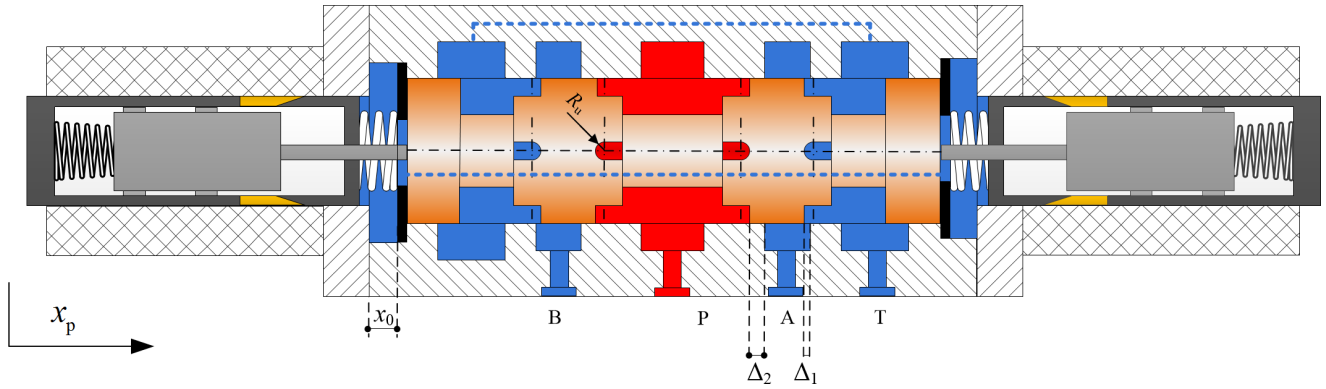

FIGURE 12. Schematic of the pilot valve.

where Δ_1 is the underlap region length of ports A and B to port T, Δ_2 is the overlap region length of port P to ports A and B, and n_{pa}, n_{pb}, n_{at}, n_{bt} are the corresponding number of the U-shape notches on P-A, P-B, A-T, B-T orifices. The corresponding structural parameters are presented in Fig. 12, and the opening area of each orifice is calculated and presented in Fig. 13.

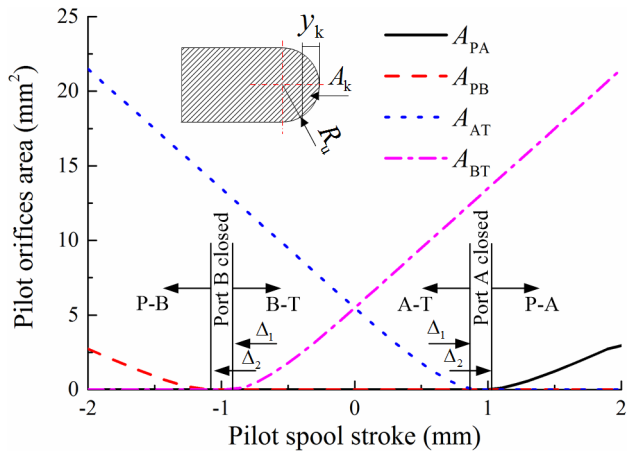

FIGURE 13. Structural parameters and opening area of the pilot valve.

The flow force acts as the main resistance to the spool movement and is important in completing the dynamic mechanical model. By considering the steady part and the dynamic part, the flow force can be defined by

$$F_{pfl}=2C_q\cos\theta_k\sum_{k=1}^{4}(A_k\Delta P_k)+C_q\frac{dx_p}{dt}\sum_{k=1}^{4}\left(V_{pk}\sqrt{2\rho\Delta P_k}\right), \tag{31}$$

where θ_k is the flow angle at each control edge, ΔP_k is the pressure differential over each orifice, and V_{pk} is the load volume between the corresponding ports. Because only the U-shape notches connect with each port within the limited displacement of the pilot spool, the notches are the main throttling structure and the load volume V_{pk} in (31) is assumed to be the corresponding volume of the notch part. Because of the small volume in the U-shape notches and relatively low velocity of the pilot spool, the dynamic flow force is very small compared to the steady flow force and is neglected in the modeling.

The pilot stage proportional valve controls the pilot flow to drive the main stage proportional valve and the resulting pilot pressure acts on the main spool to compensate the spring force and moves the spool. The pilot pressure force can be calculated by

$$F_{hy}=|P_a-P_b|A_v\mathrm{sgn}(x_m)\ \ 0\le|x_m|\le x_{mmax}, \tag{32}$$

where P_a is the pressure of the control chamber A which connects with the port A of the pilot valve, P_b is the pressure of the control chamber B which connects with the port B of the pilot valve, and A_v is the acting area of the main spool. Because of the existence of the control chamber, the compression of the oil needs to be considered for the coupling of flow and pressure. The flow continuity equation can be written as

$$\begin{cases} q_a=A_v\dfrac{dx_m}{dt}+C_{ep}P_a+\dfrac{V_a}{\beta_e}\dfrac{dP_a}{dt}, \\ q_b=A_v\dfrac{dx_m}{dt}+C_{ep}P_b+\dfrac{V_b}{\beta_e}\dfrac{dP_b}{dt}, \end{cases} \tag{33}$$

where V_a, V_b are the volume of the control chambers A and B, respectively, C_{ep} is the leakage coefficient of the chambers, and β_e is the effective volume elastic modulus.

As in the pilot valve, the flow force still acts as the main resistance force of the spool moving. Because of the large amount of complex flow controlled by the main spool, simply using the static flow force equation may cause large error. Therefore, the static flow force is indirectly measured using two pressure sensors installed separately on the pilot control chambers. The pressure differential is firstly measured when the spool is moved to a certain position without the flow, and the force equation is expressed as

$$(P_{a1}-P_{b1})A_v=k_m x_m+F_{mk0}-F_{mfs}, \tag{34}$$

where P_{a1} and P_{b1} are the pressure of the control chambers, F_{mfs} is the static friction. Then the flow can be given to the

valve to measure the flow force and the corresponding force equation can be described as

$$(P_{a2} - P_{b2})\,A_v = k_m x_m + F_{mk0} + F_{mfl} - F_{mfs}, \quad (35)$$

where P_{a2} and P_{b2} are the corresponding pressure of the control chambers. The spool under the above two conditions are both slightly moved to get the maximum static friction. From (34) and (35), the flow force can be derived as

$$F_{mfl} = (P_{a2} - P_{b2} - P_{a1} + P_{b1})\,A_v. \quad (36)$$

The static flow force is measured at P-A and A-T orifices at the pressure differential of 5 bar and the results are presented in Fig. 14. The static flow force in the simulation model is recalculated based on the measured data and the actual pressure differential.

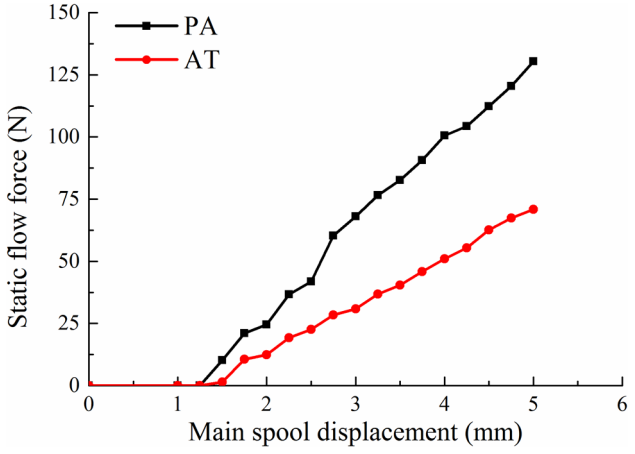

FIGURE 14. Measured static flow force at the pressure differential of 5 bar.

The dynamic flow force is quite important in modeling the dynamic response of the proportional valve. It is also modeled in (37) as a function of the spool displacement and the valve structure as that in the pilot valve.

$$F_{mfl} = C_q \frac{dx_m}{dt} \sum_{k=1}^{4} \left(V_{mk} \sqrt{2\rho \Delta P_k} \right), \quad (37)$$

where V_{mk} is the load volume of each orifice.

The load volume can be defined as (38), as shown at the bottom of this page, where L_p, L_t, L_{t1}, a, b, θ are the parameters of the valve structure, Δ_m is the overlap region length of the main spool, and h_{mt} is the depth of the trapezoidal shape notch on the spool. The above parameters are presented in Fig. 15.

E. VALVE MODELING

The subsystems are coupled with each other and form the pilot operated proportional directional valve. A block diagram which explains the relationship between each subsystem is presented in Fig. 16. The model is co-simulated with AMESim and Matlab/Simulink software.

The input control voltage signal is first transferred into PWM signal and given to the solenoids. The driving current changes correspondingly and leads to the change of the flux field in the solenoids. The electromagnetic force also changes. Then the electromagnetic force is imbalanced with the flow force and the spring force in the pilot stage and leads to the movement of the pilot spool. The displacement change of the pilot spool alters the opening area of the pilot valve and changes the pilot flow correspondingly to move the main spool. The movement of the main spool affects the pilot pressure, the spring force, and the flow force. The main spool keeps moving until the spring force and the flow force are large enough to overcome the risen pilot pressure and gains the new balanced state.

In the pilot-operated proportional directional valve, the driven current in the left and right solenoids are monitored and given back to the controller. The displacement of the main spool is measured with inductive position transducer installed on the main stage of the proportional valve and is also given back to the controller for closed loop control.

$$\begin{aligned}
V_{pa} &= \begin{cases} \left\{\left[L_p + b - (x_m + \Delta_m)\right]\left[a - 2(x_m + \Delta_m)\tan\theta\right] - \left[a - \frac{3}{2}(x_m + \Delta_m)\tan\theta\right]\frac{x_m + \Delta_m}{2}\right\} h_{mt} & -x_{m\max} \le x_m \le -\Delta_m, \\ 0, & -\Delta_m < x_m \le x_{m\max}, \end{cases} \\
V_{bt} &= \begin{cases} \left\{\left(L_t - \frac{L_{t1}}{2} + b + \frac{x_m + \Delta_m}{2}\right)\left[a - 2(x_m + \Delta_m)\tan\theta\right] - \left[a - \frac{3}{2}(x_m + \Delta_m)\tan\theta\right]\frac{x_m + \Delta_m}{2}\right\} h_{mt} & -x_{m\max} \le x_m \le -\Delta_m, \\ 0 & -\Delta_m < x_m \le x_{m\max}, \end{cases} \\
V_{at} &= \begin{cases} 0 & -x_{m\max} \le x_m < \Delta_m, \\ \left\{\left(L_t - \frac{L_{t1}}{2} + b - \frac{x_m - \Delta_m}{2}\right)\left[a + 2(x_m - \Delta_m)\tan\theta\right] + \left[a + \frac{3}{2}(x_m - \Delta_m)\tan\theta\right]\frac{x_m - \Delta_m}{2}\right\} h_{mt} & \Delta_m \le x_m \le x_{m\max}, \end{cases} \\
V_{pb} &= \begin{cases} \left\{\left[L_p + b + (x_m - \Delta_m)\right]\left[a + 2(x_m - \Delta_m)\tan\theta\right] + \left[a + \frac{3}{2}(x_m - \Delta_m)\tan\theta\right]\frac{x_m - \Delta_m}{2}\right\} h_{mt} & \Delta_m \le x_m \le x_{m\max}, \\ 0 & -x_{m\max} < x_m \le \Delta_m, \end{cases}
\end{aligned} \quad (38)$$

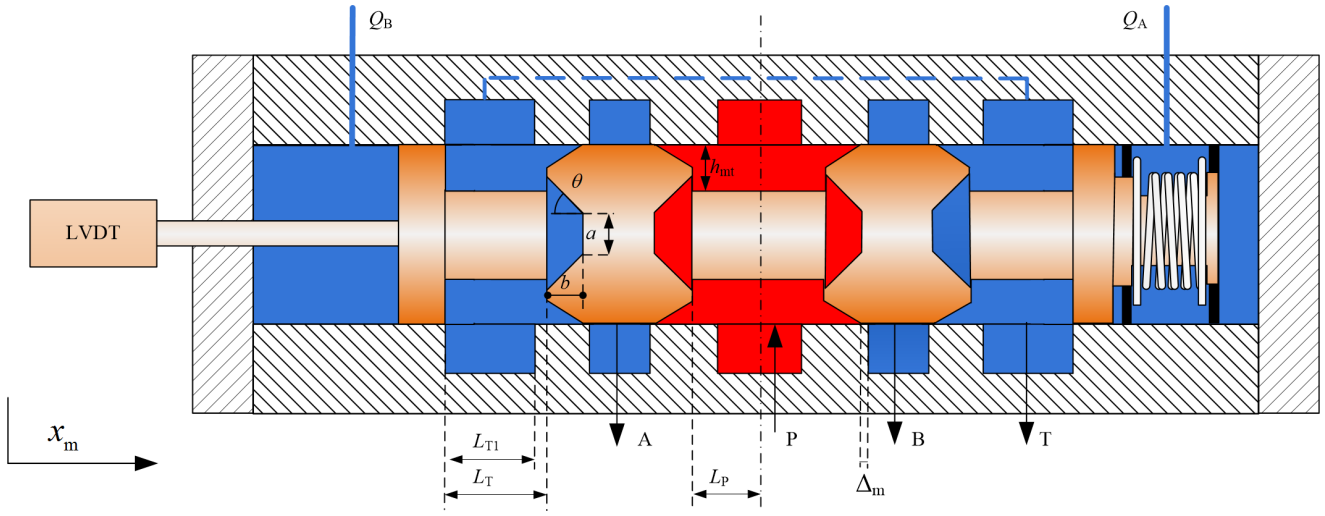

FIGURE 15. Schematic of the main valve.

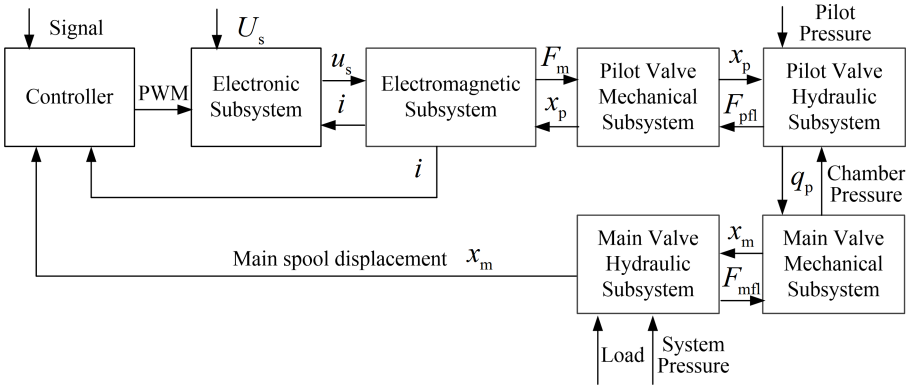

FIGURE 16. Block diagram of the pilot operated proportional directional valve subsystems.

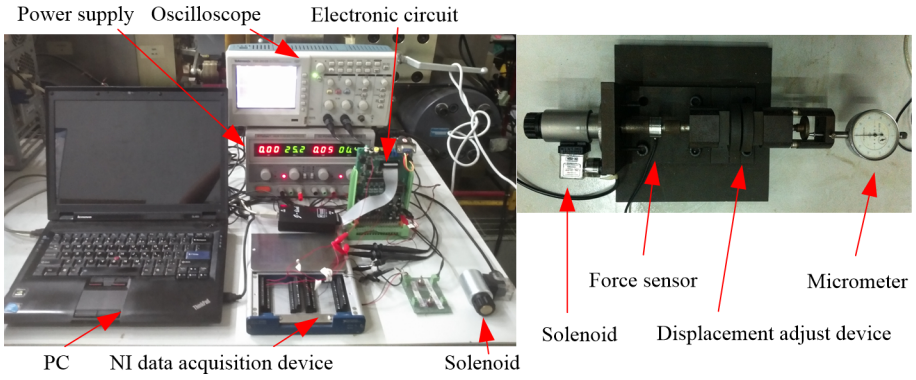

FIGURE 17. Photograph of the test rig and the solenoid test device.

In the simulation, a proportional-integral (PI) controller and a proportional-integral-derivative (PID) controller are designed to control the current and the displacement of the main spool, respectively. The parameters of the controllers are adjusted based on the real valve.

IV. VALIDATION OF THE SIMULATION MODEL

A. ELECTROMAGNETIC SUBSYSTEMS VALIDATION

The model of the electronic subsystem and the electromagnetic subsystem are built and verified by a specific test rig. The photograph of the test rig is presented in Fig. 17.

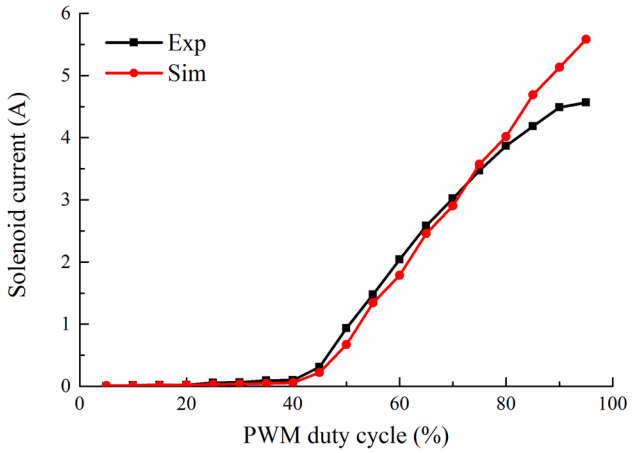

FIGURE 18. Solenoid current affected by PWM duty cycle.

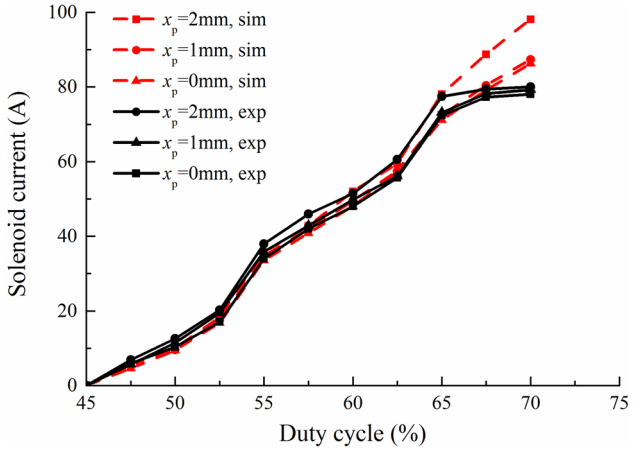

FIGURE 19. Solenoid current affected by PWM duty cycle and core displacement.

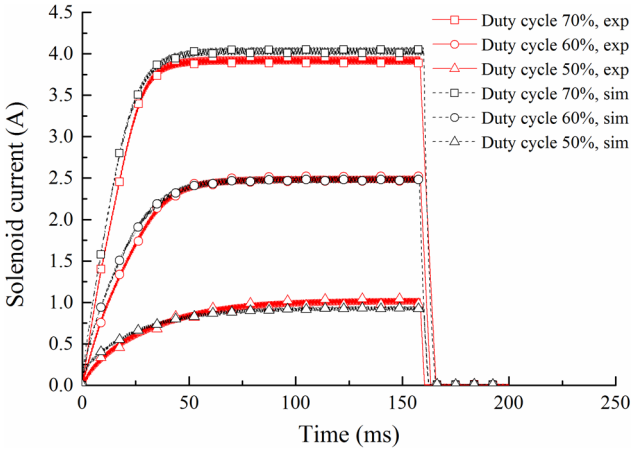

FIGURE 20. Simulated and experimental solenoid current.

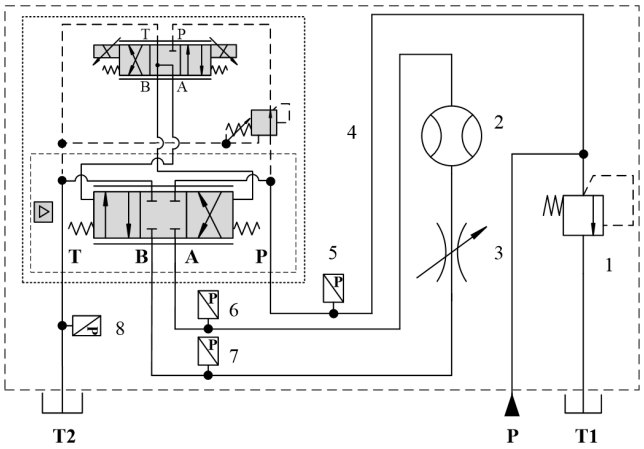

FIGURE 21. Schematic of the hydraulic test rig: 1. Relief valve 2. Flow sensor 3. Throttle valve 4.Pilot operated proportional directional valve 5.6.7.8. Pressure sensors.

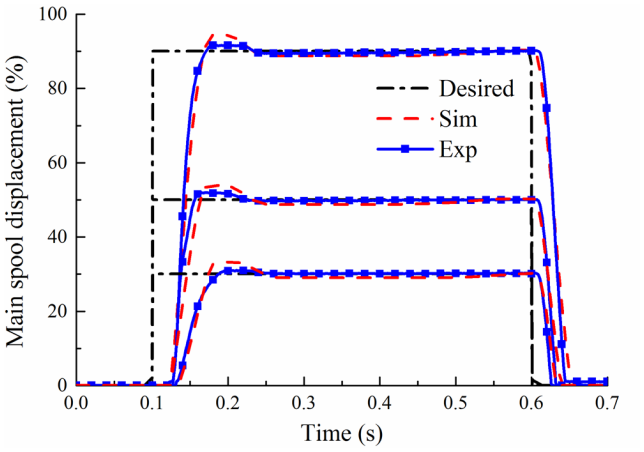

FIGURE 22. Main Spool response when the valve is given different step signals.

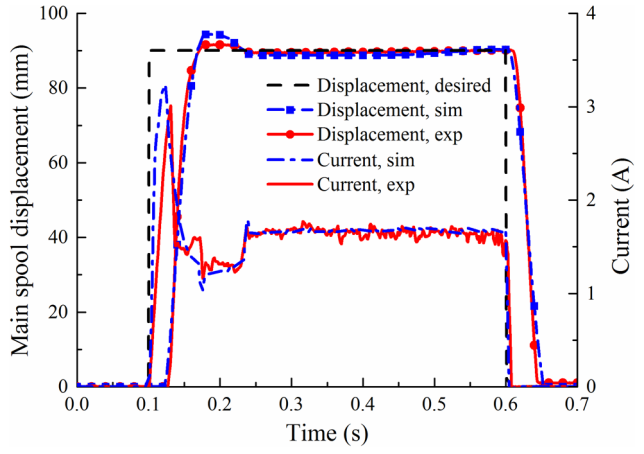

FIGURE 23. Spool displacement and solenoid current when the valve is given step signal.

The test rig mainly consists of a power supply, an oscilloscope, an electronic circuit, a PC, a NI data acquisition device, and a solenoid test device. The current signal can be observed by the oscilloscope through the sampling resistor and the generated voltage can be acquired by the NI data acquisition device. The solenoid test device consists of a force sensor, a displacement adjust device, and a micrometer.

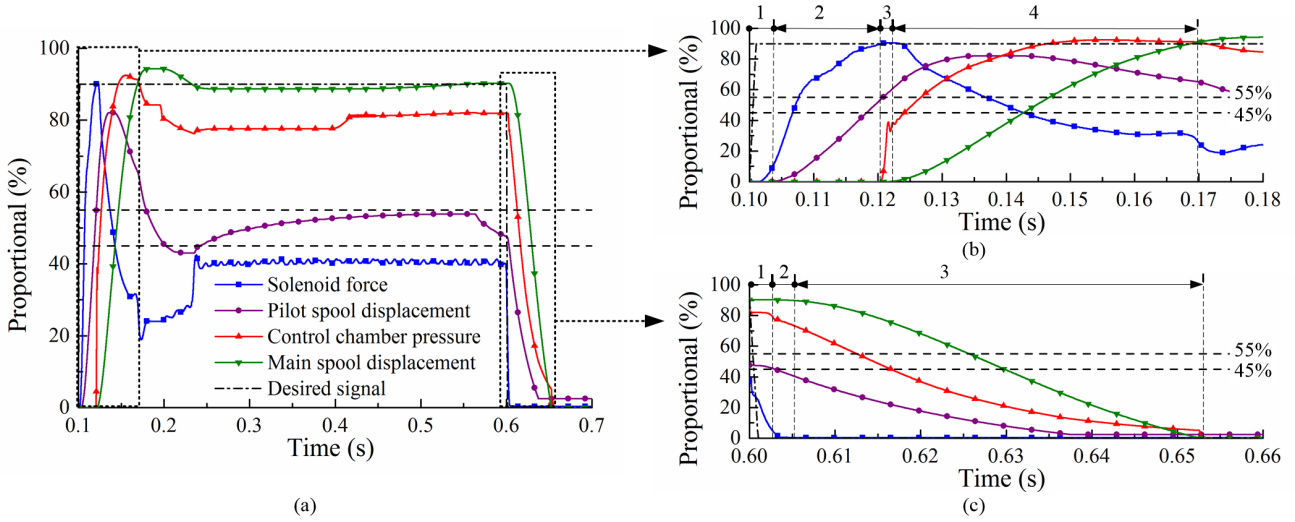

FIGURE 24. Simulation valve behaviors when the valve is given step signal: (a) full period (b) 90% step signal (c) 0 step signal.

The displacement adjust devices is a slider which can be adjusted by a screw to limit the displacement of the solenoid core.

The relationship between the duty cycle, the current, and the electromagnetic force at the static state is tested. Given the normally used 2000 Hz PWM signal, the relationship between the duty cycle and the current at the displacement of zero is presented in Fig. 18. The simulation results and the experimental results are presented in the same figure. The behavior of the model matches well with the experimental result. The limited power of the power supply constrains the performance of the solenoid in the experiment and leads to the large error when the solenoid is given large duty cycle. The relationship between the duty cycle and the current at different displacements are presented in Fig. 19. The simulation result also fits well with the experimental result and can reproduce the nonlinear behavior.

The current behavior when the solenoid is given step signal is also tested to verify the dynamic behavior of the model, and the results of simulation and experiment are presented in Fig. 20. The ascending time of the current is about 50 ms and the descending time is about 5 ms, which reflects the characteristics of the anti-unloading power drive circuit.

B. VALVE VALIDATION

To verify the above simulation model, a hydraulic test rig is used, and the schematic diagram is shown in Fig. 21. The PC with the data acquisition device is used to measure and store the pressure and the displacement data. A signal generator is used to give the desired signal to the valve. The power supply with the pressure of 10 MPa and flow rate of 200 L/min is used to power the system. The ports A and B are connected and the oil temperature is set up at $40°\pm2°$.

The comparison of the simulation and the experiment when the valve is given different desired displacement signal is presented in Fig. 22. The simulation fits the experiment well. The main spool movement is delayed at first, and then the displacement rises rapidly and a small overshoot appears. The displacement is maintained stable at the controlled value until it is given zero signal and the spool moves back to the central position. The 90% of the entire stroke experiment is taken as an example, and the displacement and the current are presented in Fig. 23. The simulation displacement and the current all match well with the experimental ones.

V. DISSCUSSION

The model built above is used to analyze the factors which cause the valve delay. The 90% stroke simulation, whose results are presented in Fig. 23, is taken as an example. When the step signal is given to the valve, the response time for which the main spool moves is 69 ms, and the delay time is about 22 ms, 32% of the opening response time. When the zero signal is given to the valve, the response time of the main spool is 53 ms, and the delay time is 5 ms, 9.4% of the closing response time. The detailed simulation results of the electromagnetic force, the pilot spool displacement, the pressure of the control chamber, and the displacement of the main spool are nondimensionalized and presented in Fig. 24.

The response when the valve is given 90% step signal is enlarged and presented in Fig. 24 (b). The entire response time of the main spool can be divided into four periods and the first three periods are the delay time. In the first period, the PWM signal is given to the circuit, and the solenoid generates the electromagnetic force. The electromagnetic force rises gradually and the pilot spool moves when the electromagnetic force is large enough to compensate the friction and the spring force. The first period is about 4 ms. In the second period, the pilot spool moves from the central position. Before the pilot spool moves to 45% of the full stroke (the underlap region length, $\Delta 1$ in Fig. 12), the control chamber still connects with the returning port. And in latter

part of this period, the pilot spool moves to 55% of the full stroke (the overlap region length, $\Delta 2$ in Fig. 12). At this time, the returning port is shut down, but the displacement is still smaller than the overlap region (dead zone) length. The pressured oil is not supplied to the control chamber and the control pressure maintains unchanged. The time needed in this period is about 16 ms. In the third period, the spool moves long enough and exceeds the dead zone to the control position. The pressure port and the control chamber are connected and the pressure in the control chamber rises. Then the pilot pressure force overcomes the spring force and moves the main spool. The time needed is about 2 ms. In the fourth period, the pilot pressure force is controlled by the pilot valve and moves the main spool to the desired position. The main spool moving time is about 46 ms. From the above analysis, the delay caused by the electronic components and the delay caused by the pilot valve dead zone are the two main components in the response delay, and the proportion of each part is about 17% and 73.2%, respectively.

The response when the valve is given 0 step signal is also enlarged and presented in Fig. 24 (c). The entire response time of the main spool can similarly be divided into three periods and the first two periods are the delay time. The pilot spool moves back to around 50% of the full stroke to realize detailed main spool position control, and the main spool is maintained at the desired position before the step signal is given. In the first period, the solenoid force decreases rapidly and the pilot spool moves back to the central position. However, because of the small displacement change as well as the asymmetrical designed pilot spool underlap and overlap regions, the control chamber is not connected with the pressure port, either the returning port. The control pressure remains nearly the same and maintains the main spool's position. This period is about 3 ms. In the second period, the pilot spool exceeds the dead zone and connects with the returning port. The control pressure decreases correspondingly. However, the pilot pressure force is not small enough and the static friction obstructs the main spool's movement. The main spool still maintains its position and the time of this period is about 2 ms. In the last period, the pilot pressure force is small enough and the main spool is driven by the flow force and the spring force to move to the central position. The movement costs about 48 ms, and the delay in the valve closure is mainly caused by the pilot valve dead zone and the main spool friction.

From the analysis, it can be obtained that in the entire action period, the delay is mainly caused by the electromagnetic force delay and the pilot valve dead zone. The relatively conservative control pressure supply and control strategy also slow down the valve response and aggravate the delay. The progress in decreasing the valve delay can be made by improving the electronic circuit, changing the pilot valve dead zone, and increasing the pilot spool velocity. However, the pilot dead zone is specially designed for valve stability and central position function, and cannot easily be changed. Therefore, most effort are

TABLE 1. Parameter descriptions and values.

Physical meaning	Symbol	Unit	Value
Electronic circuit PWM delay	t_d	s	2.60×10^{-5}
Electronic circuit equivalent resistor with high PWM	R_{on}	Ω	4.00×10^{-1}
Electronic circuit equivalent resistor with low PWM	R_{off}	Ω	6.00×10^{-1}
Supply voltage	U_s	V	2.40×10^{1}
Function coefficient	f_{11}	A/(Wb·m)	-5.46×10^{0}
Function coefficient	f_{10}	A/Wb	1.99×10^{1}
Function coefficient	f_{33}	A/(Wb^3·m^3)	3.76×10^{1}
Function coefficient	f_{32}	A/(Wb^3·m^2)	-1.87×10^{2}
Function coefficient	f_{31}	A/(Wb^3·m)	2.67×10^{2}
Function coefficient	f_{30}	A/Wb^3	1.89×10^{2}
Function coefficient	k_{s4}	(A·s)/(V·m^4)	2.01×10^{-1}
Function coefficient	k_{s3}	(A·s)/(V·m^3)	-3.73×10^{-1}
Function coefficient	k_{s2}	(A·s)/(V·m^2)	-8.74×10^{-3}
Function coefficient	k_{s1}	(A·s)/(V·m)	1.17×10^{-1}
Function coefficient	k_{s0}	(A·s)/V	1.54×10^{-1}
Function coefficient	t_{s4}	s/m^4	-8.11×10^{-2}
Function coefficient	t_{s3}	s/m^3	2.29×10^{-1}
Function coefficient	t_{s2}	s/m^2	-1.61×10^{-1}
Function coefficient	t_{s1}	s/m	-3.52×10^{-4}
Function coefficient	t_{s0}	s	5.46×10^{-2}
Function coefficient	h_{13}	N/(m^3·Wb^6)	1.14×10^{3}
Function coefficient	h_{12}	N/(m^2·Wb^6)	-2.81×10^{3}
Function coefficient	h_{11}	N/(m·Wb^6)	-1.99×10^{3}
Function coefficient	h_{10}	N/Wb^6	6.74×10^{3}
Function coefficient	h_{23}	N/(m^3·Wb^4)	-6.99×10^{4}
Function coefficient	h_{22}	N/(m^2·Wb^4)	7.66×10^{4}
Function coefficient	h_{21}	N/(m·Wb^4)	3.02×10^{5}
Function coefficient	h_{20}	N/Wb^4	-2.33×10^{5}
Function coefficient	h_{33}	N/(m^3·Wb^2)	6.57×10^{5}
Function coefficient	h_{32}	N/(m^2·Wb^2)	2.52×10^{6}
Function coefficient	h_{31}	N/(m·Wb^2)	-1.15×10^{7}
Function coefficient	h_{30}	N/Wb^2	5.78×10^{6}
Pilot spool mass	m_p	kg	4.00×10^{-2}
Pilot spool viscous coefficient	b_p	Ns/m	1.58×10^{2}
Pilot spring elastic coefficient	k_p	N/m	1.80×10^{4}
Pilot spring preload	F_{pk0}	N	1.6×10^{1}
Pilot spool stroke	x_{pmax}	m	2.00×10^{-3}
Pilot spool structure limited stroke	x_0	m	5.00×10^{-4}
Main spool mass	M	kg	4.5×10^{-1}
Main spool viscous coefficient	b_m	Ns/m	1.76×10^{1}
Main spring elastic coefficient	k_m	N/m	6.00×10^{4}
Main spring preload	F_{mk0}	N	1.80×10^{2}
Main spool stroke	x_{mmax}	m	5.00×10^{-3}
Oil density	P	kg/m^3	8.70×10^{2}
Oil dynamic viscosity	N	kg/ms	4.00×10^{-2}
Oil kinematic viscosity	H	m^2/s	4.71×10^{-5}
Fully developed turbulent discharge coefficient	C_{tu}		7.00×10^{-1}
Critical flow number	λ_{crit}		1.00×10^{2}
U-shape notch number on pilot spool P-B edge	n_{pb}		2
U-shape notch number on pilot spool P-A edge	n_{pa}		2
U-shape notch number on pilot spool B-T edge	n_{bt}		4
U-shape notch number on pilot spool A-T edge	n_{at}		4
Radius of the semi-circle of the U-shape notch	R_u	m	1.00×10^{-3}
Flow angle at each pilot valve control edge	θ_k	°	6.90×10^{1}
Underlap region length of A and B ports to T port	Δ_1	m	0.90×10^{-3}

TABLE 1. *(Continued.)* **Parameter descriptions and values.**

Overlap region length of P port to A and B ports	Δ_2	m	1.10×10^{-3}
Acting area of the main spool	A_v	m^2	6.16×10^{-4}
Control chamber leakage coefficient	C_{ep}	$m^3/(s\cdot Pa)$	1.11×10^{-13}
Control chamber A volume	V_a	m^3	1.02×10^{-5}
Control chamber B volume	V_b	m^3	1.17×10^{-5}
Effective elastic modulus	β_e	Pa	1.00×10^{9}
Main valve structural parameter	L_p	m	1.03×10^{-2}
Main valve structural parameter	L_t	m	1.56×10^{-2}
Main valve structural parameter	L_{t1}	m	1.20×10^{-2}
Overlap region length of the main spool	Δ_m	m	0.75×10^{-3}
Main spool structural parameter	A	m	7.16×10^{-3}
Main spool structural parameter	B	m	2.90×10^{-3}
Main spool structural parameter	θ	°	6.00×10^{1}
Trapezoidal shape notch depth	h_{mt}	m	6.20×10^{-3}

paid on improving the electronic circuit and the control methods [12], [16], [17], [27], [28], [33], reducing the resistance forces [22]–[25], and increasing the driving forces [14], [15], [19], [21]. In the modeling, we focus on the detailed characteristics of the driving circuit and the coupling relationship between the pilot flow and the control pressure. These features make the model very useful in predicting the performance of the valve improvement.

VI. CONCLUSION

A coupling modeling is presented for a pilot operated proportional directional valve in which the mechanical, electronic, electromagnetic, and fluid dynamic subsystems are coupled with each other. The model of each subsystem is proposed based on a LP approach. The nonlinear behavior of the subsystems during the valve functioning is discussed. The related parameters which describe the nonlinear behavior are identified and the analytical equations are proposed for reproducing.

The anti-unloading power drive circuit is carefully modeled by considering the component delay in the circuit. The nonlinear model of the solenoid is paid much attention for simulating the hysteresis performance. The discharge coefficient change and the fluid compression are used for a detailed model of the fluid coupling between the pilot directional valve and the main directional valve. The entire model of the valve works well in predicting the behavior when the valve is given certain signal.

By reviewing the simulation result, the factors which affect the main spool movement delay is analyzed and the effect proportion of the electronic parts and the structural parts are calculated. The electromagnetic force delay and the pilot valve dead zone are found out to be two main factors affecting the delay, and effort can be paid in these two factors to improve the valve response so that the retraction of the landing gears can be improved. Optimizing the electronic drive circuit and control strategies would be a future work. The methods for quick passing the pilot valve dead band would also be studied.

APPENDIX

See Table 1.

REFERENCES

[1] M. H. Sadraey, "Landing gear retraction system," in *Aircraft Design: A Systems Engineering Approach*, 1st ed. Chichester, U.K.: Wiley, 2013, pp. 527–528.
[2] S. J. Greenbank, "Landing gear—The aircraft requirement," *Proc. Inst. Mech. Eng., G, J. Aerosp. Eng.*, vol. 205, no. 1, pp. 27–34, Jan. 1991.
[3] F. Boniol and V. Wields, "The landing gear system case study," in *Proc. ABZ*, Toulouse, France, 2014, pp. 1–18.
[4] Q. Chao, J. Zhang, B. Xu, Y. Chen, and Y. Ge, "Spline design for the cylinder block within a high-speed electro-hydrostatic actuator pump of aircraft," *Meccanica*, vol. 53, nos. 1–2, pp. 395–411, Jan. 2018.
[5] J. Zhang, Q. Chao, and B. Xu, "Analysis of the cylinder block tilting inertia moment and its effect on the performance of high-speed electro-hydrostatic actuator pumps of aircraft," *Chin. J. Aeronaut.*, vol. 31, no. 1, pp. 169–177, Jan. 2018.
[6] Y. Yin, H. Nie, H. Ni, and M. Zhang, "Reliability analysis of landing gear retraction system influenced by multifactors," *J. Aircraft*, vol. 53, no. 3, pp. 713–724, May 2016.
[7] H. Khan, S. Abou, and N. Sepehri, "Fault detection in electro-hydraulic servo-positioning systems using sequential test of Wald," in *Proc. CCECE*, Winnipeg, MB, Canada, 2002, pp. 1628–1633.
[8] J. Hu, W. Wu, S. Yuan, and C. Jing, "Opening and closing of a novel high-speed switching valve," *Proc. Inst. Mech. Eng., I, J. Syst. Control Eng.*, vol. 226, no. 4, pp. 466–475, Apr. 2012.
[9] K. U. Yang, J. G. Hur, G. J. Kim, and D. H. Kim, "Non-linear modeling and dynamic analysis of hydraulic control valve; effect of a decision factor between experiment and numerical simulation," *Nonlinear Dyn.*, vol. 69, no. 4, pp. 2135–2146, Sep. 2012.
[10] N. Janse van Rensburg, J. L. Steyn, and P. S. Els, "Time delay in a semi-active damper: Modelling the bypass valve," *J. Terramech.*, vol. 39, no. 1, pp. 35–45, Jan. 2002.
[11] H.-H. Liao, M. J. Roelle, J.-S. Chen, S. Park, and J. C. Gerdes, "Implementation and analysis of a repetitive controller for an electro-hydraulic engine valve system," *IEEE Trans. Control Syst. Technol.*, vol. 19, no. 5, pp. 1102–1113, Sep. 2011.
[12] L. Schmidt and T. O. Andersen, "Application of second order sliding mode algorithms for output feedback control in hydraulic cylinder drives with profound valve dynamics," *E&I Elektrotechnik Informationstechnik*, vol. 133, no. 6, pp. 238–247, Sep. 2016.
[13] B. Magyar, C. Hős, and G. Stépán, "Influence of control valve delay and dead zone on the stability of a simple hydraulic positioning system," *Math. Problems Eng.*, vol. 2010, pp. 1–15, Jun. 2010, doi: 10.1155/2010/349489.
[14] HUSCO International, Inc. *SCX180 Valve System Solutions*. Accessed: 2011. [Online]. Available: http://www.husco-offhighway.com/products/hydraulic-control-valves-2/scx-platform/
[15] Parker Valve Division. *Series VPL Proportional Valves*. Accessed: 2004. [Online]. Available: http://ph.parker.com/us/17593/en/pressure-compensated-directional-control-valve-vpl-series
[16] F. Breidi, T. Helmus, and J. Lumkes, "The impact of peak-and-hold and reverse current solenoid driving strategies on the dynamic performance of commercial cartridge valves in a digital pump/motor," *Int. J. Fluid Power*, vol. 17, no. 1, pp. 37–47, Jan. 2016.
[17] I.-Y. Lee, "Switching response improvement of a high speed on/off solenoid valve by using a 3 power source type valve driving circuit," in *Proc. IEEE ICIT*, Mumbai, India, Dec. 2006, pp. 1823–1828.
[18] D. Cristofori and A. Vacca, "The modeling of electrohydraulic proportional valves," *J. Dyn. Syst. Meas. Control*, vol. 134, no. 2, p. 021008, Mar. 2012.
[19] X. Kong and S. Li, "Dynamic performance of high speed solenoid valve with parallel coils," *Chin. J. Mech. Eng.*, vol. 27, no. 4, pp. 816–821, Jul. 2014.

[20] Y. Zhu and B. Jin, "Analysis and modeling of a proportional directional valve with nonlinear solenoid," *J. Brazilian Soc. Mech. Sci. Eng.*, vol. 38, no. 2, pp. 507–514, Feb. 2016.
[21] B. Jin, Y. Zhu, W. Li, D. Zhang, L. Zhang, and F. Chen, "A differential control method for the proportional directional valve," *J. Zhejiang Univ. Sci. C*, vol. 15, no. 10, pp. 892–902, Oct. 2014.
[22] R. Amirante, L. A. Catalano, C. Poloni, and P. Tamburrano, "Proportional directional valves," *Eng. Optim.*, vol. 46, no. 10, pp. 1295–1314, Oct. 2014.
[23] N. Herakovič, J. Duhovnik, and M. Šimic, "CFD simulation of flow force reduction in hydraulic valves," *Tehn. Vjesnik*, vol. 22, no. 2, pp. 453–463, 2015.
[24] N. Z. Aung, J. Peng, and S. Li, "Reducing the steady flow force acting on the spool by using a simple jet-guiding groove," in *Proc. FPM*, Harbin, China, 2015, pp. 289–294.
[25] P. Bordovsky, K. Schmitz, and H. Murrenhoff, "CFD simulation and measurement of flow forces acting on a spool valve," in *Proc. IFK*, Dresden, Germany, 2016, pp. 473–484.
[26] F. Meng, H. Zhang, D. Cao, and H. Chen, "System modeling, coupling analysis, and experimental validation of a proportional pressure valve with pulsewidth modulation control," *IEEE/ASME Trans. Mechatronics*, vol. 21, no. 3, pp. 1742–1753, Jun. 2016.
[27] J. Fang, Z. Chen, and J. Wei, "Some practical improvements of sliding-mode control for servo-solenoid valve," *Proc. Inst. Mech. Eng., I, J. Syst. Control Eng.*, vol. 230, no. 7, pp. 591–609, Aug. 2016.
[28] E. Canuto and W. Acuna-Bravo, "Hierarchical digital control of a proportional electrohydraulic valve," in *Proc. ICMA*, Takamatsu, Japan, 2013, pp. 1015–1020.
[29] N. D. Vaughan and J. B. Gamble, "The modeling and simulation of a proportional solenoid valve," *J. Dyn. Syst. Meas. Control*, vol. 118, no. 1, pp. 120–125, Mar. 1996.
[30] A. Dell, "Amico and P. Krus, "Modelling and experimental validation of a nonlinear proportional solenoid pressure control valve," *Int. J. Fluid Power*, vol. 17, no. 2, pp. 90–101, May 2016.
[31] W. Wu, J. Hu, S. Yuan, and C. Di, "A hydraulic hybrid propulsion method for automobiles with self-adaptive system," *Energy*, vol. 114, pp. 683–692, Nov. 2016.
[32] J. Zhang, D. Wang, B. Xu, M. Gan, M. Pan, and H. Yang, "Experimental and numerical investigation of flow forces in a seat valve using a damping sleeve with orifices," *J. Zhejiang Univ.-Sci. A*, vol. 19, no. 6, pp. 417–430, Jun. 2018.
[33] X. Zhao, L. Li, J. Song, C. Li, and X. Gao, "Linear control of switching valve in vehicle hydraulic control unit based on sensorless solenoid position estimation," *IEEE Trans. Ind. Electron.*, vol. 63, no. 7, pp. 4073–4085, Jul. 2016.
[34] M. Ruderman and A. Gadyuchko, "Phenomenological modeling and measurement of proportional solenoid with stroke-dependent magnetic hysteresis characteristics," in *Proc. ICM*, Vicenza, Italy, 2013, pp. 180–185.
[35] H. E. Merritt, *Hydraulic Control Systems*. New York, NY, USA: Wiley, 1967, pp. 39–45.
[36] *AMEsim Hydraulic Library Manual Rev 10*, Siemens Product Lifecycle Manage. Softw. Inc., Plano, TX, USA, 2010.
[37] X. Chen, S. Shentu, D. Jin, B. Meng, and J. Ruan, "A discharge coefficient model for orifice flow based on revised Reynolds number," presented at the 9th ICFP, Hangzhou, China, Apr. 2017.

JUNHUI ZHANG received the B.S. and Ph.D. degrees in mechatronics from Zhejiang University, Hangzhou, China, in 2007 and 2012, respectively.

He is currently an Associate Research Fellow with the State Key Laboratory of Fluid Power and Mechatronic Systems, Zhejiang University. His research interests include noise reduction of hydraulic pumps/motors, fluid power components and systems, and mechatronic systems design.

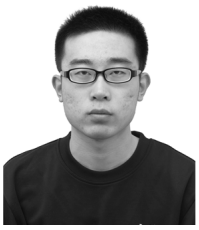

DI WANG received the B.S. degree in mechatronics from Zhejiang University, Hangzhou, China, in 2013.

He is currently pursuing the Ph.D. degree in mechatronic control engineering with Zhejiang University. His research interests include fluid power components and systems, mechatronic systems design, and fault diagnosis of the hydraulic system.

BING XU received the Ph.D. degree in fluid power transmission and control from Zhejiang University, Hangzhou, China, in 2001.

He is a Professor and a Doctoral Tutor with the School of Mechanical Engineering, Zhejiang University, where he is currently the Deputy Director of the State Key Laboratory of Fluid Power and Mechatronic Systems. He has authored or co-authored over 100 journal and conference papers. He holds 31 authorized patents. His research interests include fluid power components and systems, mechatronics systems design, energy saving, and motion control for mobile machinery. He is a Senior Member of CMES and CSAA.

ZHENYU LU received the B.S. degree in mechatronics and the M.S. degree from Nanchang University, Nanchang, China, in 2010 and 2013, respectively.

He is currently pursuing the Ph.D. degree in mechatronic control engineering with Zhejiang University, Hangzhou, China. His research interests include fluid power components and systems, motion control of hydraulic systems, and mechatronic systems design.

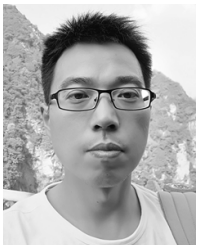

MINYAO GAN received the M.S. degree in mechanical manufacturing and automation from the Kunming University of Science and Technology, Kunming, China, in 2004.

He is currently a Senior Engineer with the Shanghai Marine Equipment Research Institute. His current research interests include marine engineering technology and hydraulic lifting system.

QI SU received the B.S. and Ph.D. degrees in mechatronics from Zhejiang University, Hangzhou, China, in 2010 and 2016, respectively.

He is currently an Assistant Engineer with the School of Mechanical Engineering, Zhejiang University. His research interests include fluid power components and systems and motion control of hydraulic systems, and mechatronic systems design.